Tertiary proton diagnostics in future inertial confinement fusion experiments

S. Cremer[a] and C. P. Verdon[b]
Laboratory For Laser Energetics, University of Rochester, 250 East River Road, Rochester, New York 14623-1299

R. D. Petrasso
Plasma Science and Fusion Center, Massachusetts Institute of Technology, Cambridge, Massachusetts 02139

(Received 27 April 1998; accepted 12 May 1998)

Recently, it was proposed to use energetic (up to 31 MeV) tertiary protons produced during the final stage of inertial confinement fusion implosions to measure the fuel areal density of compressed deuterium–tritium (DT). The method is based on seeding the fuel with ^{3}He. The reaction of ^{3}He ions with the energetic knock-on deuterons, produced via the elastic scattering of 14.1 MeV neutrons, is a source of very energetic protons capable of escaping from very large areal density targets. This work presents results of detailed time-dependent Monte Carlo simulations of the nuclear processes involved in producing and transporting these protons through imploding targets proposed for direct-drive experiments on OMEGA [D. K. Bradley *et al.*, Phys. Plasmas **5**, 1870 (1998)] and the National Ignition Facility [S. W. Haan *et al.*, Phys. Plasmas **2**, 2480 (1995)]. [S1070-664X(98)03510-1]

I. INTRODUCTION

Future inertial confinement fusion (ICF) experiments at the National Ignition Facility (NIF) in the U.S.A.[1] and at the MegaJoule Laser Facility in France[2] are expected to achieve near-burn conditions. For such experiments copious amounts of neutrons (more than 10^{18}) will be emitted, which, on their way out from the capsule, will give birth, via secondary and tertiary processes, to relatively large amounts of charged-particle species. From all these particle species, the most energetic will be tertiary protons, capable of escaping and conveying information on the compressed target conditions.[3]

In a DT target seeded with ^{3}He, tertiary protons are born in the ''in-flight'' fusion reactions of either knock-on deuterons with background ^{3}He, or from knock-on ^{3}He with background deuterons. In either case, the knock-ons are produced by elastic scattering from 14.1 MeV neutrons. On the experimental side, it is proposed to measure the high-energy part of the tertiary escaping proton spectrum with a new charged-particle spectrometer under development at the OMEGA facility.[4]

Charged particles have been successfully used to measure areal density. For example, primary 3.02 MeV protons[5] and secondary 12.5–17.6 MeV protons[6] were used to measure relatively modest values of ρR (up to 10 mg/cm^2) in pure deuterium targets; and deuteron and triton knock-ons were used to measure fuel areal density in compressed DT targets,[7] for cases with total areal density (fuel+pusher) up to 100 mg/cm^2. The present work will show than even a modestly driven OMEGA DT gas target, for which the fuel (ρR) is about 40 mg/cm^2 and the pusher ($\rho \Delta R$) about 150 mg/cm^2, the tertiary proton method may be required to make a reliable measurement of the time-averaged fuel areal density.

To explore the utility of the tertiary proton method, this paper will focus on three cases: A gas capsule implosion on OMEGA (Sec. III A); an OMEGA cryogenic implosion (Sec. III B); and a NIF cryogenic implosion that ignites and burns (Sec. III C). To investigate these cases, we utilize a one-dimensional (1D) hydrocode (LILAC) that steps through the evolution of the imploding targets. At each time step, a Monte Carlo code (IRIS) simulates tertiary and other nuclear processes.

II. THE TERTIARY PROTON SOURCES

Tertiary protons are produced in an ICF DT target seeded with ^{3}He via two different, but very much alike, channels. First, the primary 14.1 MeV neutrons produced by the thermonuclear reaction

$$\mathrm{D+T}\rightarrow n(14.1\ \mathrm{MeV})+\alpha(3.5\ \mathrm{MeV}), \tag{1}$$

are elastically scattered by the deuterons and ^{3}He plasma ions, producing knock-on deuterons (D*) and ^{3}He* with energies up to 12.56 and 10.63 MeV, respectively

$$n+\mathrm{D}\rightarrow n'+\mathrm{D}^* \tag{2}$$

and

$$n+{}^3\mathrm{He}\rightarrow n'+{}^3\mathrm{He}^*. \tag{3}$$

The above two reactions are anisotropic, having 15.7% (or 13.5%) of the total knock-on deuterons (or ^{3}He) produced with energies in the range of 9.7–12.56 MeV (or 7.5–10.63 MeV). The total cross sections for the above two reactions are $\sigma_{d1}=0.62$ barn and $\sigma_{h1}=1.00$ barn, respectively.

Similar to the reaction (3), the 14.1 MeV neutrons may elastically scatter off the plasma tritons (T), producing triton

[a]Permanent address: Rafael Ballistic Center, Haifa, PO Box 2250, Israel 31021.
[b]Presently at Lawrence Livermore National Laboratory, Livermore, CA 94551.

TABLE I. The initial configurations of the OMEGA and NIF capsuls.

Case	Capsule type	Outer diameter	Gas fill	Fuel-layer thickness	CH-Ablator thickness
1	OMEGA Gas	750 μm	10 atm DT	350 μm DT gas	25 μm
2	OMEGA Cryo	880 μm	~0.1 atm ^{3}He	90 μm DT ice	3 μm
3	NIF Cryo	3400 μm	~0.1 atm ^{3}He	344 μm DT ice	3 μm

knock-ons (T*) with a distribution similar to that of the ^{3}He*. The total cross section for this reaction is $\sigma_{t1} = 0.92$ barn.

The most-energetic knock-ons D* and ^{3}He* may interact in flight with the deuterons and the ^{3}He plasma ions, producing tertiary protons with energies up to 30.76 and 28.90 MeV, respectively

$$D^* + {}^3He \rightarrow \alpha + p(30.76\ \text{MeV}) \tag{4}$$

and

$${}^3He^* + D \rightarrow \alpha + p(28.90\ \text{MeV}). \tag{5}$$

Alternatively, when D*'s or T*'s fuse with plasma tritons or deuterons, very energetic tertiary neutrons are also produced, with energies up to 30.1 and 28.2 MeV, respectively.[8] (This different diagnostic case will not be discussed further.)

The Q value for the reactions (4) or (5) is 18.3 MeV. The cross sections for the reaction (4) are slowly decreasing from $\sigma_{d2} = 47-43$ mbarn, when the energy of D* increases over its high-energy domain (9.7–12.56 MeV). The cross sections for the reaction (5) are slowly decreasing from $\sigma_{h2} = 57-51$ mbarn when the energy of ^{3}He* increases over its high-energy domain (7.5–10.63 MeV).

Based on the cross section considerations only, the total number of tertiary protons born via ^{3}He*-channel [Eqs. (3) and (5)] will be $(1.00/0.62)*(54/45) = 1.94$ times larger than the total number of tertiary protons born via the knock-on deuterons channel [Eqs. (2) and (4)]. In addition, reactions (4) and (5) are anisotropic and forward directed. For example, 50% of all the tertiary protons produced via reaction (4) will have their energies in the range of 27.68–30.76 MeV.

If the temperatures inside the fuel (or at least inside the region that contains ^{3}He) are sufficiently high, the knock-on deuterons will not range out before ''sampling'' the average areal density of the region. In such a case, the fuel (ρR) can be related to the number of tertiary protons produced (with energy above some minimum limit, $E_{\min}$). Specifically

$$Y_P^d \sim F_d * f_D * \sigma_{d1} * f_{He} * \sigma_{h2} * (1/M_{\text{eff}})^2 * Y_N * (\rho R)^2 \tag{6}$$

and

$$Y_P^h \sim F_h * f_{He} * \sigma_{h1} * f_D * \sigma_{d2} * (1/M_{\text{eff}})^2 * Y_N * (\rho R)^2, \tag{7}$$

where M_{eff} is the average atomic mass, Y_N is the total primary 14.1 MeV neutron yield, f_D and f_{He} are the atomic fraction of deuterium and ^{3}He, and F_d and F_h are numerical factors that depend on the detailed anisotropy of Eqs. (2)–(5), relative to the minimum energy $E_{\min}$.

In the case that Eqs. (6) and (7) hold, the ratio of the total number of tertiary protons produced $(Y_P^d + Y_P^h)$ to the total number of primary neutrons produced $(Y_N) - R_{T/P}$ (tertiary over primary) will be proportional to the square of the fuel areal density.

If, on the other hand, the temperatures are not sufficiently high or the fuel (ρR) values are very large, the knock-on deuterons and ^{3}He will range out before sampling the whole fuel areal density. In this case, the effective power of (ρR) in relations (6) and (7) will approach the value one. In this limit the proportionality to (ρR) arises from the initial knock-on production processes only. The second (ρR) term in the above relations is replaced by the average range of the knock-on D's and ^{3}He, according to the actual values of the temperature in the target.

The above considerations are valid when dealing with a static-like situation. However, during burn the thermodynamic conditions inside the compressed target change, such that the number of tertiary protons escaping from an imploding target needs to be related to a moving time average of its areal fuel density, with the neutron rate used as a weighting factor. Herein, the time dependence of the ''neutron-weighted,'' moving time-averaged fuel areal density will be given by

$$\langle \rho R \rangle_{nw}(t) = \Sigma[(\rho R)_i * Y_N^i] / \Sigma[Y_N^i], \tag{8}$$

the summation being done for the evolving time steps (i) during the burn, until time t.

Since the fusion neutron velocities are much larger than the material velocities, the simulation of the above processes can be done only for a relatively small number of IRIS time steps which, therefore, are effectively much coarser than the hydrodynamic ones. The size of IRIS time intervals is chosen in such a way to correctly mimic the time history of the primary neutron rate.

III. THE MAIN RESULTS

The initial configuration of the cases treated in this work are given in Table I. The OMEGA gas capsule consists of a relatively thick CH-ablator shell filled with DT gas. The cryogenic capsules consist of a spherical shell of DT ice encapsulated by a very thin CH-ablator shell. The initial ^{3}He fill for the cryogenic capsules will be such that, after evaporation of DT ice at the inner shell and compression, it will eventually obtain, at peak burn, approximately a 25% concentration for the OMEGA case and about a 5% concentration for the NIF case.

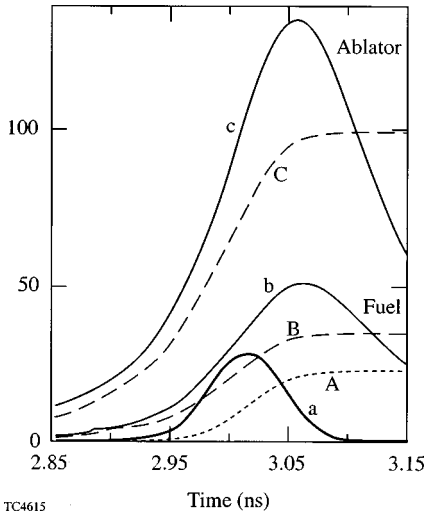

FIG. 1. The burn history of the OMEGA gas capsule as calculated by the hydrocode LILAC: The primary fusion neutron rate (10^{13}/ns) (a) and yield (10^{12}) (A); the fuel (b) and the CH-ablator (c) areal densities (mg/cm^2), together with their neutron-weighted counterparts (B) and (C), respectively.

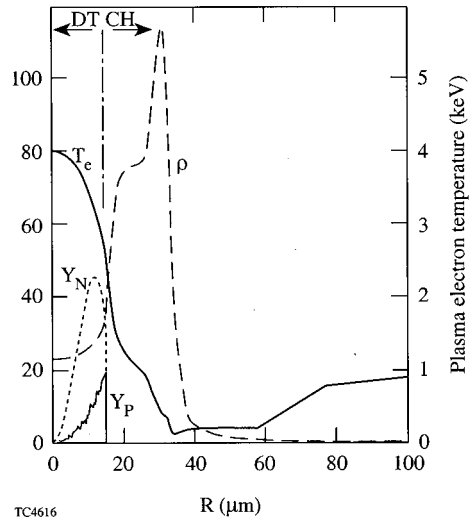

FIG. 2. OMEGA gas capsule at peak burn time (see Fig. 1). Radial profiles of the mass density ρ [left axis (g/cm^3)] and of the plasma electron temperature T_e [right axis (keV)]. Also depicted (left axis) are the radial profiles of the primary neutron yield Y_N (in units of 10^9) and the associated tertiary proton source Y_P.

For the one-dimensional LILAC simulations, we assumed an incident 351 nm laser pulse. The total energy on the target is 30 kJ for the OMEGA and 1.5 MJ for the NIF capsules. The pulse shape was designed to put the imploding capsule on an $\alpha_a=3$ isentrope[9] (α_a being a parameter that measures the departure from the Fermi degenerate pressure near the ablation surface). This particular design ameliorates the development of a strong Rayleigh–Taylor instability during the implosion, a consequence of which would be to lower by more than an order of magnitude the expected primary neutron yield. Overall, the design approach taken herein implies that the calculated yield will probably not exceed the experimental yield by more than a factor of 5–10.

Since the total number of tertiary protons produced [by both channels, Eqs. (6) and (7)] is proportional to the product

$$f_D \cdot f_T \cdot (f_D \cdot f_{He} + f_{He} \cdot f_D) = 2 \cdot f_D^2 \cdot f_T \cdot f_{He},$$

the f's being the atomic fraction of these species, the optimal choice for the D:T:^{3}He atomic fractions to maximize the tertiary proton production is 2:1:1, with $f_{He}=0.25$.

A. The OMEGA gas capsule case

Figure 1 summarizes the burn history of the primary neutron rate and yield for the OMEGA gas-capsule case, the time history of the fuel and of the pusher areal densities, and their ''neutron-weighted'' counterparts as defined by the relation (8). As can be seen, the limiting value of $\langle \rho R \rangle_{nw}$ is 35 mg/cm^2 for the fuel and 100 mg/cm^2 for the CH shell. Their maximum values at peak compression are 47% and 38% higher, respectively, than their neutron-weighted counterparts. Figure 2 depicts the mass density profile at the peak neutron rate (3.019 ns), together with the plasma electron temperature profile, T_e. Figure 2 depicts also the radial distribution of the primary neutron source (in units of 10^9), and (by the shaded area) the distribution of the tertiary proton source evaluated for an IRIS time interval (of 7.25 ps) around the peak burn time. Figure 3 describes the evolution of the time-integrated escaping tertiary proton spectrum, at peak burn and at the end of the burn, for energies above the secondary (D–^{3}He) proton energy limit (17.6 MeV). These latter protons are produced by secondary fusion reactions of the 0.82 MeV ^{3}He nucleons (originating from one branch of the DD primary fusion reaction) with the plasma deuteron ions.

Energy integration of these spectra provide the total number of escaping tertiary protons at different times during the burn. The ratio of this number to the total number of primary neutrons produced at the respective stage—$R_{T/P}$ (tertiary over primary)—is plotted in Fig. 4 against the instantaneous fuel areal density values $(\rho R)_F$, or against the moving, time-averaged neutron-weighted $\langle \rho R \rangle_{nw}$. During

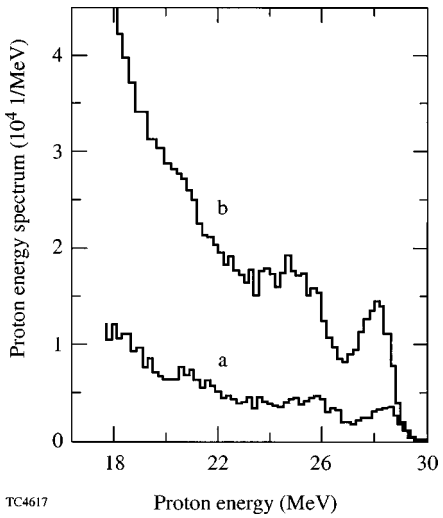

FIG. 3. OMEGA gas capsule. The evolution of the time-integrated escaping tertiary proton spectra at peak burn (a), and at the end of the burn (b) (see Fig. 1).

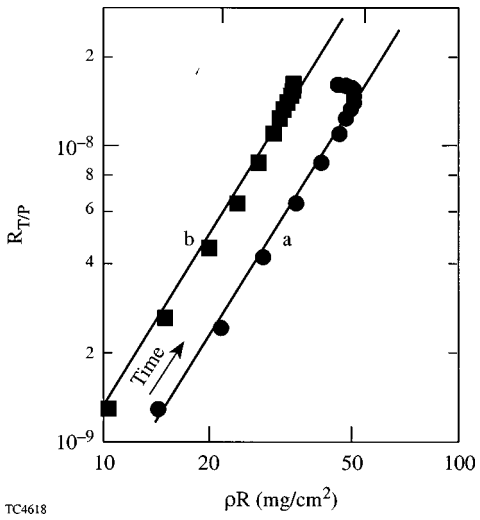

FIG. 4. OMEGA gas capsule implosion. The evolution of the ratio $R_{T/P}$, as a function of (a) the instantaneous fuel areal density $(\rho R)_F$; (b) the neutron-weighted fuel areal density $\langle \rho R \rangle_{nw}$.

the first part of the burn, until peak compression, $R_{T/P}$ is seen to be proportional to the square of $(\rho R)_F$. As we pass the maximum compression, this simple proportionality begins to fail. Most importantly, however, the left curve (b), which plots $R_{T/P}$ versus $\langle \rho R \rangle_{nw}$, remains proportional to the square of $\langle \rho R \rangle_{nw}$ until the very last stages of the burn. This curve connects the effective values of fuel areal densities during the burn with the calculated (and eventually measured) value of the ratio $R_{T/P}$. A simple relation can be written for this case

$$R_{T/P} = 1.25 * 10^{-11} * \langle \rho R \rangle_{nw}^2, \tag{9}$$

with $\langle \rho R \rangle_{nw}$ given in mg/cm^2. It is worthwhile to note that, in this instance, Eq. (9) predicts a tertiary peak yield that is a factor of about 3 smaller than the qualitative yield predictions of Eqs. (6) and (7).

While the number of knock-on deuterons produced in this target is almost 4.5 orders of magnitude larger than the number of tertiary protons, these deuterons are unobservable since, in this case, they are ranged out in the ablator (see Fig. 2).

B. The OMEGA cryo-DT capsule

A cryo-DT capsule consists of a solid (ice)-DT shell, covered by a thin shell of plastic (CH ablator). Table I presents the initial configuration of such a capsule designed for future OMEGA experiments. To achieve ignition, the void inside the solid-DT shell can be filled with a small amount of DT gas, or as an alternative, one can rely on the inherent DT gas accumulated at the center of the target as a result of the evaporation of some small portion of the inner part of the solid-DT shell. The role of this central gaseous zone in future igniting target designs is to help reach the high temperatures and the minimum fuel areal density needed to assure a strong central ignition and a consequent propagating macroscopic burn.

Figure 5(a) presents the mass density and the plasma

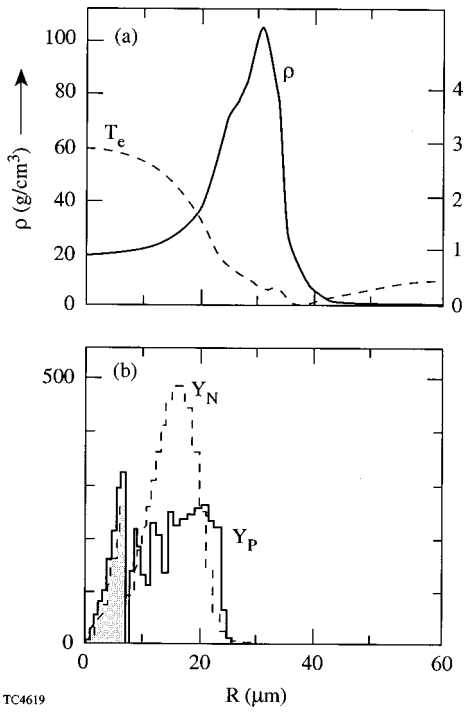

FIG. 5. OMEGA cryo-DT capsule at peak burn time: (a) The mass density (ρ) and the electron temperature (T_e) profiles; (b) the radial distribution of the primary neutron yield Y_N (dotted line, in units of 10^9) and of the associated tertiary proton (with $E > 23$ MeV) source, Y_P (full line); shaded area—the D*'s channel contribution only [see Eq. (6)].

electron temperature profiles for the OMEGA cryo-DT imploded target at the peak burn time, as calculated by the LILAC code. This capsule, having a very thin initial CH shell, allows the laser to burn through it, ablating as well a part of the solid-DT shell. Consequently, the compressed target configuration consists of only a thick pure-DT shell, with a small part of its central gaseous DT zone (8 μm in Fig. 5) seeded with ~25% (atomic) ^{3}He. According to the one-dimensional hydrocode simulations, the areal density of the seeded zone will reach, at the peak burn, an instantaneous value of 16 mg/cm^2, while the corresponding instantaneous total areal density of the fuel reaches 180 mg/cm^2. The dotted line in Fig. 5(b) depicts the radial distribution of the primary neutron yield (in units of 10^9); the full line in Fig. 5(b) depicts the radial distribution of the tertiary protons (with energy above 23 MeV) produced during an IRIS time step (of 12.8 ps). The shaded area under the full curve depicts the tertiary protons' radial profile produced within the ^{3}He-seeded region by knock-on deuterons only, and, as can be seen, this is the major source of tertiary protons produced in the seeded region.

Knock-on deuterons produced outside the seeded region can be approximately ignored because of kinematic considerations or because they range out before they can interact with ^{3}He in the seeded region.

On the other hand, the ^{3}He knock-ons produced inside the seeded region will dominantly fuse with the plasma deuterons outside the seeded zone. This is because the areal density of the seeded zone of this capsule is much lower than the needed value to range out the energetic ^{3}He* nucleons.

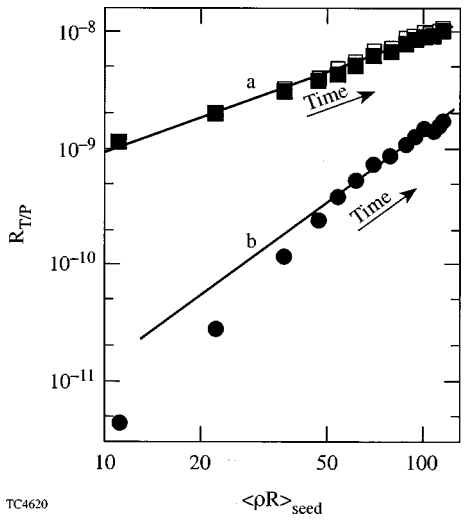

FIG. 6. OMEGA cryo-DT capsule. (a) The evolution of the ratio $R_{T/P}$ as a function of the areal density of the central seeded region (from two different Monte Carlo runs); (b) the contribution of the D*'s channel only.

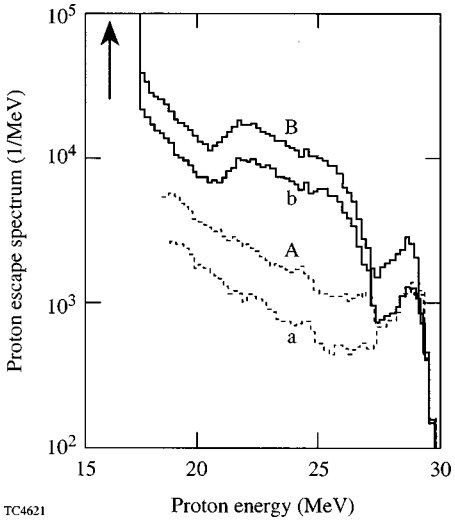

FIG. 7. OMEGA cryo-DT capsule. The evolution of the time-integrated escaping tertiary proton spectra from the peak burn time (b), up to the end of the burn (B). The dotted histograms (a,A) depict the D*'s channel contribution only.

In this instance, calculations show that about five times as many tertiary protons are produced outside than inside the seeded zone.

Figure 6 depicts the evolution of the ratio $R_{T/P}$ for the escaping tertiary protons with the energy above 17.6 MeV. The abscissa is the moving neutron-weighted, time-averaged areal density of the seeded region. For comparison, we present in the same figure the contribution coming from the D* channel only. Except for the first stages of the burn, the ratio for D*-channel contribution is proportional to the square of the areal density of the seeded zone, as expected. On the other hand, for all tertiary protons produced, most of which are generated outside the seeded zone, the ratio is, to a very good approximation, proportional to the first power of the time-averaged neutron-weighted areal density of the seeded zone during all stages of the burn (see the upper dotted line in Fig. 6).

A simple relation for the upper dotted line of Fig. 6 is

$$R_{T/P} = 9 * 10^{-10} * \langle \rho R \rangle_{\text{seed}}, \tag{10}$$

with the seeded areal density given in mg/cm^2.

Beside the contribution of the cross section factors, the constant in the relation (10) is proportional to the range needed to slow down the most energetic ^{3}He knock-ons to energies below 4 to 5 MeV. For the present study this range is about 60–70 mg/cm^2, a value which remains relatively constant during the whole burn period. Other scenarios for the fuel temperature will require some adjustment in this ''constant.''

Figure 7 depicts the time-integrated escaping-tertiary-proton-energy spectrum at the peak burn time and at the end of the burn. It is worth emphasizing that the production of very-high-energy tertiary protons can be simply related to the square of the areal density of the seeded region, without any need of a detailed knowledge of the existing temperatures inside the fuel during the burn. In such instance, since the high-energy-peak (hep) in Fig. 7 contains 4220 protons (with escape energy above 28 MeV), while the total primary neutron yield of the capsule is 2.8×10^{13}, we have $R_{T/P}$ (hep) $=1.5\times10^{-10}$. By using the value of the neutron-weighted areal density of the seeded region, 11.5 mg/cm^2, we conclude that

$$R_{T/P}(\text{hep}) = 1.15\times10^{-12}\langle \rho R \rangle^2_{\text{seed}}, \tag{11}$$

with $\langle \rho R \rangle_{\text{seed}}$ in mg/cm^2. We remark that for this particular case, the hep contribution comes mainly from the knock-on deuterons produced inside the seeded region.

It is interesting to note that the implosion of the OMEGA cryo-DT target has the property that, during the whole burn process, the areal density of the seeded zone is almost proportional to total fuel areal density, the latter being approximately ten times larger. Therefore, the time-averaged values of these two quantities will preserve the same proportionality, and by inferring one of them (i.e., that of the seeded zone) we can approximate the other by simply multiplying the inferred value by the above calculated factor. This property is a consequence of the hydrodynamic (one-dimensional) self-similarity of the implosion process, a property that can be affected, in real situations,by growth of asymmetries during the last stages of the implosion.

C. The NIF cryo-DT target

The future NIF laser is expected to deliver 1.5 MJ ultraviolet (UV) energy on the target. Table I provides the initial configuration data for a (gain$=$25) cryo-DT capsule, directly driven by the NIF laser. Dealing with an igniting and macroscopically burning target, we assume the central region at the burn time has only 5% ^{3}He, a fraction considered small enough not to interfere with the ignition process.[3]

Figure 8 presents the time history of the areal density of the whole fuel and of the seeded region only, together with the time history of the primary neutron rate. Since, in this case, the macroscopic burn period is very short relative to the entire implosion period, the time-averaging process of the

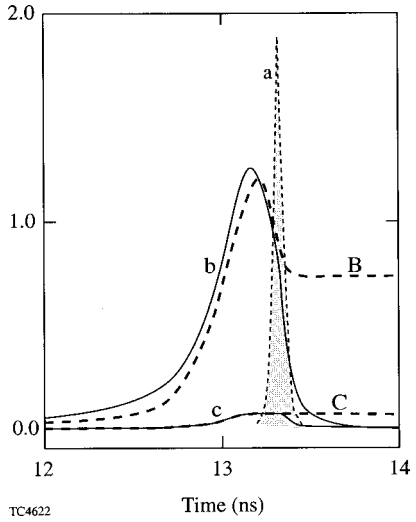

FIG. 8. The burn history of the NIF cryo-DT (gain=25) capsule. (a) The primary fusion neutron rate (shaded area, in units of 10^{29}/s); the instantaneous total (b) and the seeded region only (c) fuel areal densities (g/cm^2), together with their neutron weighted counterparts (B and C, respectively).

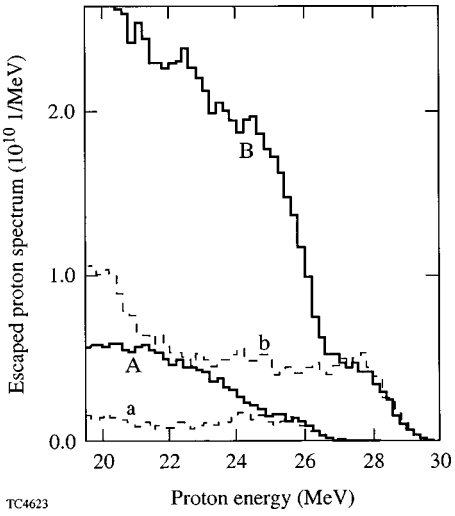

FIG. 9. NIF cryo-DT capsule. The time-integrated escaped-tertiary-protons spectra at peak burn time (A) and at the end of the burn (B). The dotted histograms (a) and (b) represent, respectively, the contribution of the D*'s channel only (as calculated in a different Monte Carlo run).

areal density by the primary neutrons [see Eq. (8)] will mainly project out the ρR values at the peak burn time. The values of $\langle \rho R \rangle_{nw}$, evaluated by expression (8), are depicted in Fig. 8 by the thick dotted lines.

In addition to the depletion of the main fuel during the burn, the simulation of the secondary and tertiary processes involved in the production of the tertiary protons in such a target will have to take into account the accumulation of ^{3}He inside the fuel. These nucleons, produced via the primary reaction

$$\mathrm{D}+\mathrm{D}\rightarrow n(2.45\ \mathrm{MeV})+{}^3\mathrm{He}(0.82\ \mathrm{MeV}), \tag{12}$$

slow down and stop in the plasma, enriching the fuel with a considerable amount of ^{3}He.

Since, in principle, knock-on deuterons and knock-on ^{3}He are produced all over the fuel, it will be possible to have reactions of the types (3) and (4) in any part of the capsule. Since the temperatures in the central region are much higher, the accumulation of ^{3}He inside the seeded region are even larger, and, in fact, at the end of the burn the atomic concentration of ^{3}He inside the seeded region is almost 7%, relative to the 5% concentration at the beginning of the burn.

Because of these complications, a simple relation between tertiary protons and fuel ρR may be difficult to establish for an ignited NIF capsule. However, the spectrum of the tertiary protons (see Fig. 9), as observed from different directions, will still potentially convey very useful information about the symmetry of the implosion, i.e., differences in the tertiary proton spectrum and yield can be related to differences in ρR along that line of sight, a circumstance in which the penetrating power of the very energetic tertiary proton is exploited.

Also, for the unignited NIF capsules—both gas and cryogenic—we conjecture that a simple proportionality is likely to exist between the number of escaped tertiary protons and fuel ρR, in a fashion similar to the OMEGA case studies presented herein.

ACKNOWLEDGMENTS

The authors thank D. Shvarts for helpful suggestions during the writing of this manuscript.

This work was supported by the U.S. Department of Energy (DOE) Office of Inertial Confinement Fusion under Cooperative Agreement No. DE-FC03-92SF19460, the University of Rochester, and the New York State Energy Research and Development Authority. The support of DOE does not constitute an endorsement by the DOE of the views expressed in this paper.

[1] S. W. Haan, S. M. Pollaine, J. D. Lindl *et al.*, Phys. Plasmas **2**, 2480 (1995).
[2] D. Butler, Nature (London) **375**, 6 (1995).
[3] R. D. Petrasso, C. K. Li, M. D. Cable *et al.*, Phys. Rev. Lett. **77**, 2718 (1996).
[4] D. G. Hicks, C. K. Li, R. D. Petrasso *et al.*, Rev. Sci. Instrum. **68**, 589 (1997).
[5] Y. Kitagawa, K. A. Tanaka, M. Nakai *et al.*, Phys. Rev. Lett. **75**, 3130 (1995).
[6] H. Azechi, N. Miyanaga, R. O. Stapf *et al.*, Appl. Phys. Lett. **49**, 555 (1986); see also H. Azechi, M. D. Cable, and R. O. Stapf, Laser Part. Beams **9**, 119 (1991).
[7] S. Skupsky and S. Kacenjar, J. Appl. Phys. **52**, 2608 (1981); S. Kacenjar, S. Skupsky, A. Entenberg, L. Goldman, and M. Richardson, Phys. Rev. Lett. **49**, 463 (1982).
[8] D. R. Welch, H. Kislev, and G. H. Miley, Rev. Sci. Instrum. **59**, 610 (1988); see also Laboratory for Laser Energetics LLE Review **69**, 46, National Technical Information Service Document No. DOE/SF/19460-152 (1996). Copies may be obtained from the National Technical Information Service, Springfield, VA 22161.
[9] J. D. Lindl, Phys. Plasmas **2**, 3933 (1995).